Anti-Stokes excitation of solid-state quantum emitters for nanoscale thermometry

Tran, Toan Trong; Regan, Blake; Ekimov, Evgeny A.; Mu, Zhao; Zhou, Yu; Gao, Wei-bo; Narang, Prineha; Solntsev, Alexander S.; Toth, Milos; Aharonovich, Igor; Bradac, Carlo

2019

https://hdl.handle.net/10356/106464

https://doi.org/10.1126/sciadv.aav9180

Anti-Stokes excitation of solid-state quantum emitters for nanoscale thermometry

Toan Trong Tran[1]*, Blake Regan[1], Evgeny A. Ekimov[2], Zhao Mu[3], Yu Zhou[3], Wei-bo Gao[3], Prineha Narang[4], Alexander S. Solntsev[1], Milos Toth[1], Igor Aharonovich[1], Carlo Bradac[1]*

Color centers in solids are the fundamental constituents of a plethora of applications such as lasers, light-emitting diodes, and sensors, as well as the foundation of advanced quantum information and communication technologies. Their photoluminescence properties are usually studied under Stokes excitation, in which the emitted photons are at a lower energy than the excitation ones. In this work, we explore the opposite anti-Stokes process, where excitation is performed with lower-energy photons. We report that the process is sufficiently efficient to excite even a single quantum system—namely, the germanium-vacancy center in diamond. Consequently, we leverage the temperature-dependent, phonon-assisted mechanism to realize an all-optical nanoscale thermometry scheme that outperforms any homologous optical method used to date. Our results frame a promising approach for exploring fundamental light-matter interactions in isolated quantum systems and harness it toward the real- ization of practical nanoscale thermometry and sensing.

INTRODUCTION

Stokes and anti-Stokes emission are fundamental phenomena widely used to study the physicochemical and optical properties of materials. Stokes (anti-Stokes) photoluminescence (PL) occurs when the energy of the emitted photons is lower (higher) than that of the absorbed ones. In the anti-Stokes case, the extra energy that causes upconversion of the photons can be acquired through a variety of mechanisms, ranging from multiphoton absorption (1) to Auger recombination (2) and phonon absorption (3). The latter, relevant to this work, is illustrated in Fig. 1 (A and B). A photon with energy $h\nu_{exc}$ at the long-wavelength tail of the absorption spectrum excites an electron from a thermally populated first vibronic state ($n_0 = 1$) of the electronic ground state E_0 to the bottom manifold ($n_1 = 0$) of an excited electronic state E_1 (red arrow). The system can then return to the ground state via spon- taneous emission of an upconverted photon with a ZPL energy $h\nu_{se} > h\nu_{exc}$ (yellow arrow). This phonon-assisted anti-Stokes excitation process scales exponentially with temperature and is the bedrock of a variety of fundamental studies [e.g., cavity quantum electro- dynamics (4)], as well as practical applications such as optical cryo- cooling (5), bioimaging (6), and Raman spectroscopy (7). However, anti-Stokes PL is inherently inefficient, and all work done to date on solid-state defects has been focused on ensembles (8, 9) rather than individual point defects.

Here, we demonstrate that anti-Stokes PL can be used to study iso- lated quantum systems—specifically atom-like color centers in dia- mond, over a large range of temperatures. We explore the mechanism for some of the most studied diamond defects, the nitrogen-vacancy (NV) (10), the silicon-vacancy (SiV) (11), and the germanium-vacancy (GeV) (12) centers. We show that anti-Stokes excitation of selected di- amond color centers is an efficient process, detectable by standard PL spectroscopy, and leverage this finding to demonstrate upconversion

PL from a single isolated GeV defect. We show that the anti-Stokes excitation process is thermally activated and proceeds through a phonon-photon absorption pathway rather than through multi- photon absorption. We exploit the high anti-Stokes excitation effi- ciency to introduce an innovative approach for all-optical nanoscale thermometry based on the temperature dependence of the anti-Stokes to Stokes PL intensity ratio. Our technique outperforms all other pre- viously reported all-optical nanothermometry methods.

RESULTS

To frame the scope of the anti-Stokes process for quantum emitters and its capacity for developing nanoscale sensing applications, we characterized diamond samples (see Methods) containing GeV, SiV, and NV centers. A schematic illustration of a diamond defect in the split-vacancy configuration (i.e., GeV and SiV) is shown in Fig. 1B. For each of the diamond defects, we selected a specific pair of excitation lasers (see Methods and fig. S1) with energies above (Stokes) and be- low (anti-Stokes) the ZPL of each emitter. Figure 1 (C to E) shows room temperature Stokes (blue) and anti-Stokes (ocher) PL spectra for ensembles of GeV, SiV, and NV centers, respectively. Note that the sharp edges of the emission peaks are due to band-pass filters used to suppress the excitation lasers. The insets show the complete Stokes PL spectra of each color center. At room temperature, all color centers show anti-Stokes PL. To confirm that the upconversion was not caused by multiphoton absorption, we measured PL intensity versus excitation power and concluded that the scaling does obey one-photon rather than two-photon absorption dynamics (see fig. S2).

Next, we established a direct, quantitative comparison among the anti-Stokes to Stokes PL ratios of the studied centers. Normalizing the anti-Stokes intensity makes the comparison independent of the den- sity of defects among the different samples. The comparison does, nonetheless, issue some caveats. The first regards the selection of the Stokes and anti-Stokes laser excitation wavelengths. Our hypothesis is that the anti-Stokes excitation process involves vibronic states of the defects, which are populated via the absorption of phonons by ground- state electrons. It therefore follows that the process depends on the pho- non spectral density, i.e., the phonon density of states multiplied by the transition amplitude [and can involve multiple phonons (13)], making

[1]School of Mathematical and Physical Sciences, University of Technology Sydney, Ultimo, NSW 2007, Australia. [2]Institute for High Pressure Physics, Russian Acade- my of Sciences, Moscow, Troitsk 108840, Russia. [3]Division of Physics and Applied Physics, School of Physical and Mathematical Sciences, Nanyang Technological University, Singapore 637371, Singapore. [4]John A. Paulson School of Engineering and Applied Sciences, Harvard University, Cambridge, MA, USA.
*Corresponding author. Email: trongtoan.tran@uts.edu.au (T.T.T.); carlo.bradac@ uts.edu.au (C.B.)
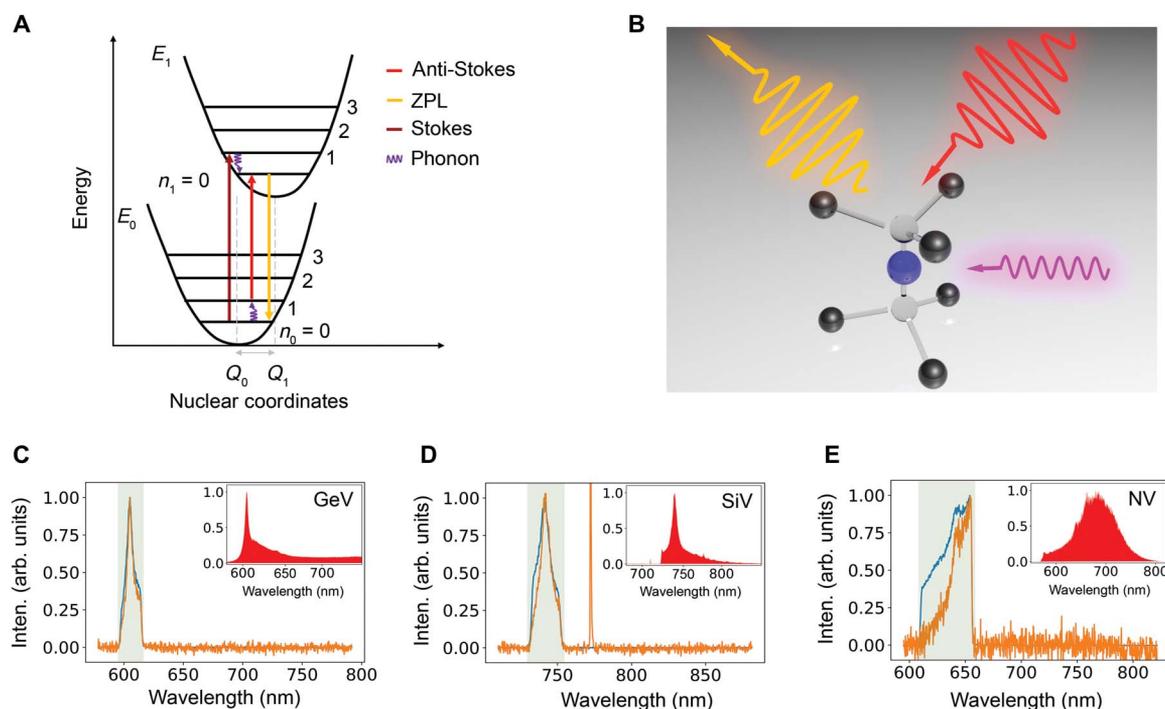
Fig. 1. Stokes and anti-Stokes luminescence processes for color centers in diamond. (**A**) Energy diagram of representative electronic and vibrational energy levels for a diamond color center. The arrows show the lower (higher) energy of the Stokes (anti-Stokes) photons with respect to the ZPL energy. In the anti-Stokes case, the additional energy is acquired via phonon(s) absorption. (**B**) Artistic representation of the anti-Stokes mechanism for a diamond color center, which absorbs a lower-energy photon (wavy line, red) and emits a higher-energy one (wavy line, ocher) upon absorption of a phonon (wavy line, purple). (**C** to **E**) PL spectra of the ZPL for nanodiamond GeV (C), SiV (D), and NV (E) centers under Stokes (blue) and anti-Stokes (ocher) excitation (the full PL spectrum under Stokes excitation is shown in the relative inset). The ZPLs (605 nm for GeV, 739 nm for SiV, and 639 nm for NV) are spectrally filtered by means of band-pass filters (semitransparent rectangular boxes). For each measurement in (C) to (E), the powers of the Stokes and anti-Stokes excitation lasers are the same: PL intensities are normalized to unity for display purposes: The measured values for anti-Stokes to Stokes PL intensity ratios for GeV, SiV, and NV centers are $I_{AS}/I_S|_{GeV} = (8.4 \pm 3.3) \times 10^{-2}$, $I_{AS}/I_S|_{SiV} = (13.2 \pm 1.1) \times 10^{-2}$, and $I_{AS}/I_S|_{NV} = (11.9 \pm 2.8) \times 10^{-5}$. The line at ~770 nm in (D) is the anti-Stokes excitation laser. The Stokes/anti-Stokes excitation wavelengths are 532/637 nm for (C), 637/770 nm for (D), and 532/720 nm for (E).

anti-Stokes absorption ideally the most efficient for excitation wavelengths matching the density maximum—and desirably not too narrow, spectrally. Note that for most color centers in solids, the phonon side band is primarily tied to the local vibrations associated with the defect. However, the dynamics of the vibrational bath can be complex and involve individual and overlapping modes, which may decay rapidly into quasi-local and global, long-wavelength, acoustic phonon modes at the femtosecond-to-picosecond time scales (*14–16*). Simultaneously, for the comparison to be meaningful, the difference between anti-Stokes and Stokes excitation energies should be similar for the different color centers. Further, for practical sensing realizations, one must ultimately consider the number of color centers per unit volume of diamond realistically achievable for each type of defect—as this affects the signal-to-noise ratio and thus the resolution of the sensor.

Bearing these caveats in mind, we find that SiV and GeV centers outperform NV centers under our experimental conditions—their anti-Stokes emission efficiency is higher as is their attainable density of defects per nanodiamond (*17*). The measured anti-Stokes to Stokes PL intensity ratios are similar for GeV and SiV centers and approximately three orders of magnitude higher than that for NV centers: $I_{AS}/I_S|_{GeV} = (8.4 \pm 3.3) \times 10^{-2}$, $I_{AS}/I_S|_{SiV} = (13.2 \pm 1.1) \times 10^{-2}$, and $I_{AS}/I_S|_{NV} = (11.9 \pm 2.8) \times 10^{-5}$. The lower efficiency of the anti-Stokes process for the NV center is somewhat counterintuitive. The NV center displays a large phononic side band, which trivially suggests more effi-

cient coupling to the lattice and a more efficient anti-Stokes excitation process compared to that of the spectrally narrower SiV and GeV centers. The much lower value of the ratio I_{AS}/I_S for the NV in our experiment is mainly due to the anti-Stokes excitation laser being quite far below the NV ZPL energy (224.40 meV) at the long-wavelength tail of the phonon side band. Additional contributing factors to the low PL anti-Stokes emission are the NV photo-ionization process (*18*) and the recently proposed NV-N tunneling mechanism in nitrogen-rich diamond samples (*19*)—hinted by the difference between the Stokes and anti-Stokes PL spectra seen in Fig. 1E.

The SiV and GeV centers have similar anti-Stokes emission efficiencies (normalized to their respective Stokes ones), making them both good candidates for anti-Stokes quantum measurements and potential nanothermometry applications (see fig. S3). However, owing to the fact that its excited state decay is highly nonradiative (*20*), the SiV center has a lower luminescence quantum efficiency than the GeV (*12*). A high quantum efficiency is desirable for it maximizes the PL signal-to-noise ratio, which ultimately determines the temperature and spatial resolution in nanothermometry. We, therefore, selected the GeV center as our primary candidate for the remainder of this work.

We start by demonstrating that anti-Stokes PL measurements are feasible down to a single quantum emitter (i.e., a single atom-like defect). Figure 2 shows the systematic analysis for the GeV center. Figure 2A is a 25 μm × 25 μm confocal PL scan of a single-crystal

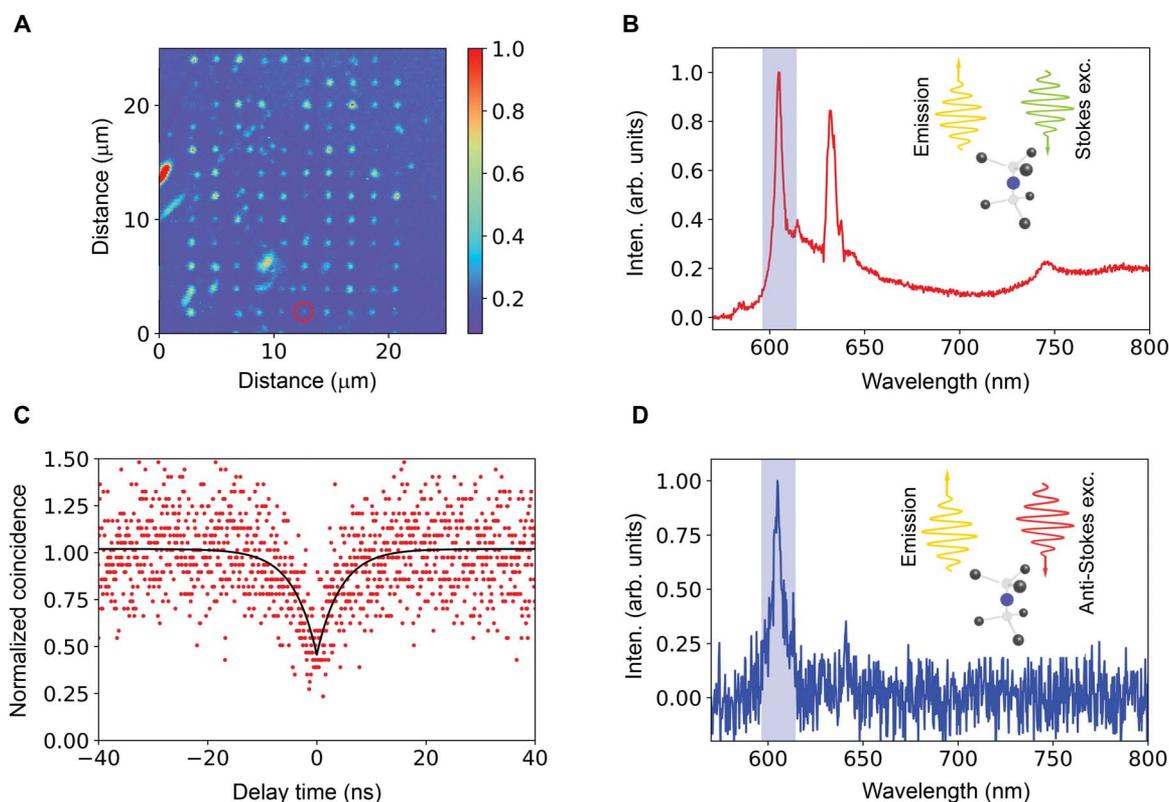**Fig. 2. Characterization of anti-Stokes emission from GeV color centers.** (**A**) Confocal image of a 25 μm × 25 μm bulk diamond sample showing emission from GeV color centers. Each spot has a different density of GeVs. The spot indicated by red circle is a single-photon GeV center as per analysis in (C). (**B**) PL spectrum acquired for the single center identified in (A). (**C**) Second-order autocorrelation function $g^{(2)}(\tau)$ showing the sub-Poissonian statistic, at zero-delay time, indicative of a single photon source, $g^{(2)}(0) < 0.5$ [the value for $g^{(2)}(0)$ is not background-corrected]. (**D**) Anti-Stokes PL spectrum acquired from the single GeV center in (A). The acquisition was carried out for 12 min, with laser excitation at 637 nm and 38 mW (23 MW/cm²) of power. A band-pass filter (represented as a semitransparent box around the ZPL of the spectrum) was used to acquire measurements in (C) and (D). The excitation wavelength used in (A) to (C) is 532 nm. The Stokes/anti-Stokes excitation wavelengths used in (D) are 532/637 nm.

diamond, where the bright spots are areas that have been implanted to induce the inclusion of GeV centers (see Methods). In the surveyed confocal scan, we isolated single GeV centers—like the one highlighted by a dashed red circle in Fig. 2A. Figure 2B shows the PL measurement of the defect. The ZPL is clearly visible at 602 nm. The quantum nature of the emitter is shown by the second-order autocorrelation function $g^{(2)}(\tau)$, which has a zero-delay time value $g^{(2)}(\tau = 0) < 0.5$ (not background-corrected)—considered indicative of a single-photon emitter (Fig. 2C). Only the ZPL signal (shaded in blue in Fig. 2B) was used for the antibunching measurement.

Next, we carried out anti-Stokes excitation of the identified GeV center. The process is efficient enough that anti-Stokes emission from a single GeV defect can be detected in a standard PL measurement. Figure 2D shows the anti-Stokes signal from the single GeV center from Fig. 2A under laser excitation at a wavelength of 637 nm, a power of 38 mW (23 MW/cm²), and a total acquisition time of 12 min. This result is notable on its own: It demonstrates, for the first time, anti-Stokes PL from a single solid-state defect.

The high efficiency of the GeV anti-Stokes PL process makes it a compelling candidate for all-optical nanothermometry (*21*). The measurement with a single center demonstrates the ultimate potential of the approach—yet practical applications can rely on ensemble measurements. Given the high density of color centers currently achievable in diamond (in parts per million), a nanoparticle just a few tens of

nanometers in size can produce bright emission for fast (in seconds) and high spatially resolved (in nanometers) temperature measurements. To quantify the sensitivity, resolution, and range of a potential nanothermometer, we characterized the Stokes and anti-Stokes PL signals from a nanodiamond (~400 nm) hosting an ensemble of GeV centers (see fig. S4), as a function of temperature. The nanodiamond GeV ensemble had a room temperature PL intensity of ~10⁶ counts/s, measured under 532-nm (Stokes) laser excitation at 500 μW (0.44 MW/cm²), after a 595- to 615-nm band-pass filter.

Figure 3A shows the results for the anti-Stokes excitation analysis (see also figs. S5 and S6). The intensity of the anti-Stokes emission exhibits Arrhenius-type exponential scaling with temperature. The data fit very well the equation $Ae^{-(E_a/k_B T)}$, with k_B being the Boltzmann constant and E_a being the value for the activation energy fixed at 102.96 meV—which is the difference in energy between the anti-Stokes excitation laser and the GeV ZPL. The Arrhenius-type dependence shows that the anti-Stokes excitation process is thermally activated, supporting our hypothesis that the anti-Stokes excitation of diamond color centers involves the absorption of phonons from the lattice.

Notably, the existence of an exponential dependence between anti-Stokes PL intensity and temperature makes the mechanism ideal for high-sensitivity nanothermometry. For the purpose of realizing a practical sensor, we use the ratio between anti-Stokes and Stokes PL as the experimental observable. The normalization makes the sensor
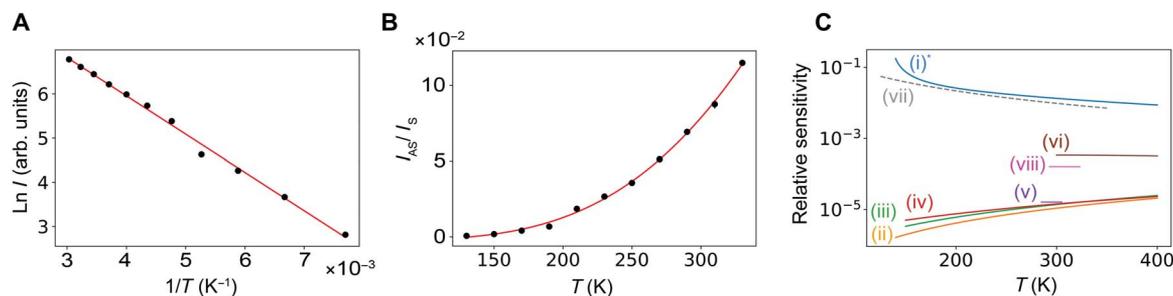
Fig. 3. Characterization of the anti-Stokes GeV-based nanothermometer. (**A**) Temperature dependence of the PL intensity signal upon anti-Stokes excitation (637-nm wavelength). The PL intensity was measured by monitoring the GeV's ZPL (605 nm) isolated with a band-pass filter. The data fit well the Arrhenius-type equation $Ae^{-(E_a/k_BT)}$, where the activation energy E_a = 102.96 meV is fixed to coincide with the difference in energy between the excitation laser and the GeV's ZPL. (**B**) Plot of the anti-Stokes to Stokes PL ratio as a function of temperature. The ratio fits an exponential curve: $a + be^{-[c/(T-T_0)]}$, granting the method an extremely high sensitivity. The error bars of plots in (A) and (B) are represented as vertical blue bars and are mostly equivalent to or smaller than the size of the data points. (**C**) Relative sensitivity plotted versus temperature for several different systems: our $I_{AS}/I_S|_{GeV}$ measurement (i)*, the frequency shift of the GeV ZPL in our Stokes PL spectra (ii), the equivalent measurement from the literature (iii), the ZPL wavelength shift of the SnV (iv) and of the SiV center (v), the intensity of the NV ZPL (vi), the Raman I_{AS}/I_S ratio achieved for a bulk thermometer (vii), and the spectral shift of quantum dots (viii). The literature data are plotted over the entire temperature range demonstrated in each paper. The excitation wavelength used in (A) is 637 nm. The Stokes/anti-Stokes excitation wavelengths used in (B) are 532/637 nm.

independent of experimental specificities (e.g., loss of detected photons due to absorption or scattering in certain environments like living cells, or samples that change phase during a heating/cooling measurement). Figure 3B shows the anti-Stokes to Stokes PL intensity ratio as a function of temperature, measured over the range of 110 to 330 K. Over this range, the I_{AS}/I_S ratio fits well the exponential function $a + be^{-[c/(T-T_0)]}$. The strong dependence on temperature is highly advantageous, as it translates to extremely high sensitivity—based on the standard definition of sensitivity, as an absolute quantity that describes the smallest amount of detectable change in a measurement. The thermometer sensitivity matches (or far exceeds) that of any other all-optical method (Fig. 3C), including techniques based on Raman spectroscopy, which boast high sensitivity over a broad temperature range (22) but are not suitable for nanoscale thermometry because they suffer from limited spatial resolution.

DISCUSSION

In terms of temperature resolution, the performance of the nanothermometer we investigated is comparable with the current best all-optical–based methods (23–25), with a noise-floor temperature resolution of 455 mK·Hz$^{-\frac{1}{2}}$ at room temperature. Note that because of the exponential dependence of the I_{AS}/I_S ratio with temperature, the resolution worsens at low temperatures yet improves rapidly at high temperatures. Specifically, in the range of 110 to 330 K, the measured temperature resolution is 2.494 to 0.420 K·Hz$^{-\frac{1}{2}}$. Unlike sensitivity, resolution is a relative quantity and can be improved, for instance, by selecting nanodiamond hosts with a higher density of color centers or by reducing the measurement bandwidth, i.e., increasing the integration time for the PL signal. For completeness, nanoscale thermometry that exploits the magnetic spin transition of diamond NV centers has been shown to reach resolutions on the order of mK·Hz$^{-\frac{1}{2}}$ (26). However, the method requires microwave excitation and may induce heating—which is undesirable in certain cases, e.g., biological environments. Moreover, even extremely small, non–quasistatic magnetic and electric fields can cause shifts in the NV spin resonance, which are potentially indistinguishable from those induced by temperature changes (27), thus limiting the accuracy of the technique in practical applications.

To complete the discussion, we benchmark the characteristics and performance of our nanothermometer against those of the current field's best. The first factor is utility. Our approach is an all-optical, microwave-free nanothermometry technique based on diamond color centers. Nanothermometers of this type (23–25) are broadly appealing because of their high spatial resolution, low noise floor (i.e., high temperature resolution), wide temperature range, and broad applicability. The second metric is sensitivity, where all-optical nanothermometers often do not perform as well, for many rely on measuring the temperature dependence on observables such as ZPL frequency (23–25) or amplitude (28), which vary weakly compared to the anti-Stokes to Stokes emission intensity ratio demonstrated here. We also note that techniques based on measuring PL intensity amplitude (rather than ratio), such as that of the NV center ZPL (28), have limited applicability because they suffer from a range of artifacts such as changes in photon scattering and absorption caused by changes in temperature of the measured sample.

Our approach is not compromised by any of these shortcomings. The anti-Stokes to Stokes PL ratio in diamond color centers reaches temperature sensitivities that match those of Raman-based sensors, while retaining the desirable utility features of the methods based on photoluminescent nanodiamonds, including a few-nanometer spatial resolution, as it works on single color centers that are stable in sub–10-nm nanodiamonds (17). Note also that the exponential scaling with temperature of the ratio I_{AS}/I_S makes the resolution of our method increase rapidly at high temperature. This makes it desirable, for instance, for temperature sensing in high-power electronics (29)—in virtue as well of diamond color centers being able to withstand extremely high temperatures (~1000 K). We add that the performance of our sensor can be further improved by carefully selecting the anti-Stokes excitation laser to match the wavelength(s) where the phonon spectral density of the color center (GeV, SiV, NV, etc.)—and thus its absorption cross section—is the highest.

Figure 3C visually captures the superior performance of our approach against other nanothermometry schemes. The graph shows an absolute comparison by plotting the relative sensitivity of each technique as a function of temperature. We define the relative sensitivity as $(\partial O/\partial T)/O$, where O is the measured observable (e.g., ZPL frequency and ZPL amplitude). The graph shows the relative sensitivity based

on (i) our anti-Stokes to Stokes PL intensity ratio, (ii) the frequency shift of the GeV ZPL in our Stokes PL spectra, equivalent to (iii) the same measurement reported in the literature (24), (iv) the ZPL wavelength shift of the SnV (25) and (v) SiV (23) diamond color centers, and (vi) the intensity change of the NV ZPL in diamond (28). The sensitivity of our technique is superior to that of any of these competitive methods; it matches (or slightly outperforms) the relative sensitivity benchmark of (vii) the anti-Stokes to Stokes emission intensity ratio of a sensor based on Raman spectroscopy (22). For reference, there is an entire family of nanothermometers (30–32) based on the temperature-varying properties of quantum dots—Fig. 3C shows an example based on (viii) spectral shift (30)—yet these are often limited to a narrow temperature range (31, 32). The nanothermometry landscape also includes upconversion nanoparticles (33–35). In some cases (33), they can reach sensitivities comparable to that of our approach, but they usually suffer from limited range of operative temperatures and/or by low quantum efficiency (i.e., low resolution). We note that the anti-Stokes method can, in principle, be applied to other systems including organic molecules (36) and carbon nanotubes (37) so long as they operate above cryogenic temperatures.

In conclusion, we have demonstrated anti-Stokes PL from a single atom-like defect in diamond and leveraged the process to demonstrate a new variant of all-optical nanothermometry with unprecedented performance. Our approach forms a basis for fundamental studies of solid-state quantum systems via anti-Stokes processes and for novel noninvasive sensing technologies.

Note added in proof: during the review process we became aware of the following work by M. Fukami *et al.* (arXiv:1903.01605 2019).

METHODS

Samples

The NV sample consisted of synthetic type Ib nanodiamond powders (MSY, ≤0.1 μm; Microdiamant) purified by nitration in concentrated sulfuric and nitric acid (H_2SO_4-HNO_3), rinsed in deionized water, irradiated by a 3-MeV proton beam at a dose of 1×10^6 ions/cm^2, and annealed in vacuum at 700°C for 2 hours to induce the formation of NV centers (Academia Sinica, Taipei, Taiwan) (38). The measured nanodiamond average size is 150.5 ± 23.3 nm.

The SiV sample consisted in nanodiamonds synthesized using a microwave plasma chemical vapor deposition (MPCVD) system from detonation nanodiamond seeds (size, 4 to 6 nm). The growth was carried out for 30 min in a gas mix of hydrogen/methane (100:1) at 900-W microwave power and 60-torr pressure. The synthesized nano-diamonds had sizes of ~0.3 to 1 μm.

For GeV centers, we looked at different samples. The first consisted of GeV centers synthesized using an MPCVD method, whereby the germanium was introduced externally as a solid or vapor source. The sample for the single GeV color centers is a high-purity single-crystal diamond from Element Six [N] <1 part per billion implanted with germanium ions at 35 keV using a nanoFIB system (ionLINE, Raith Nanofabrication) and an implantation dose of 100 Ge$^+$ ions per spot. The sample was subsequently annealed at 1000°C for 30 min in high vacuum.

The second consisted in diamond nanoparticles hosting GeV color centers synthesized from mixtures of adamantane, $C_{10}H_{14}$ (purity, >99%; Sigma-Aldrich), with small amount of tetraphenylgermanium, $C_{24}H_{20}Ge$ (purity, >95.5%; Sigma-Aldrich), at 9 GPa and 1500 to 1700 K, as described elsewhere (39). The concentration of Ge in the growth system was about 0.4% calculated relative to the carbon-germanium mixture, Ge/(Ge + C).

The third sample was a diamond membrane embedded with GeV color centers and was prepared as follows. The GeO_2-covered membrane was placed in an MPCVD chamber, along with a ~1 mm × 1 mm piece of metallic germanium ~1 cm away. The conditions were as follows: hydrogen/methane ratio of 100:1 at 60 torr and microwave power of 900 W for 10 min to fabricate a ~400-nm intrinsic diamond layer that contains GeV color centers. The diamond membranes were then flipped 180° and thinned by an inductively coupled plasma reactive ion etching (ICP-RIE) with argon, oxygen, and SF6 etch (2:3:1) at a pressure of 45 mtorr, with a forward power of 500 and 100 W for the ICP and RIE, respectively.

Optical characterization

The samples were mounted on a three-dimensional piezostage (ANPx series, attocube Inc.) in a laboratory-built, open-loop cryostat (adapted from a ST500 cryostat, Janis) with flowing liquid nitrogen. The temperature at the sample was controlled via a cryogenic temperature controller (335, Lakeshore). Optical access to the sample is through a thin quartz window; the lasers are focused via a high–numerical aperture objective (NA, 0.9; 100×; TU Plan Fluor, Nikon), back-collected, spectrally filtered, and sent to either a spectrometer (SR303I, mounted with a Newton DU920P charge-coupled device camera, Andor) or a pair of avalanche photodiodes (SPCM-AQR-14, PerkinElmer) in a Hanbury-Brown and Twiss interferometer configuration (40). Stokes/anti-Stokes excitation was carried out with the following lasers.

GeV sample

Stokes excitation was carried out with a continuous-wave (CW) diode-pumped solid-state (DPSS) laser (SDL-532-200T, Dream Lasers) at 532 nm. Anti-Stokes excitation was carried out with a TO Can laser diode (HL63142DG, Thorlabs) at 637 nm. For the anti-Stokes excitation on a single GeV defect (Fig. 3D), a short-pass dichroic was used to increase the excitation and collection efficiency.

SiV sample

Stokes excitation was carried out with a TO Can laser diode (HL63142DG, Thorlabs) at 637 nm. Anti-Stokes excitation was carried out with a CW titanium:sapphire laser (SolsTiS, M2 Inc.) at 770 nm.

NV sample

Stokes excitation was carried out with a CW DPSS laser (SDL-532-200T, Dream Lasers) at 532 nm. Anti-Stokes excitation was carried out with a picosecond gain-switched laser diode (PiL607X, PILAS) operating in CW at 675 nm and with a CW titanium:sapphire laser (SolsTiS, M2 Inc.) at 720 nm.

Thermometry

We measured the ZPL PL intensity under Stokes and anti-Stokes excitation and determined the relative anti-Stokes PL efficiency for each defect, which ultimately limits the sensitivity of the nanothermometer.

SUPPLEMENTARY MATERIALS

Supplementary material for this article is available at http://advances.sciencemag.org/cgi/content/full/5/5/eaav9180/DC1

Fig. S1. Emission and absorption spectrum for GeV, SiV, and NV centers.

Fig. S2. One- and two-photon absorption fit of the fluorescence signal measured for GeV emitters as a function of input power.

Fig. S3. Temperature dependence of PL intensity signal from SiV centers upon anti-Stokes excitation.

Fig. S4. Summary of some of the physical and optical properties of the nanodiamond sample used in this study.

Fig. S5. Overview of the variation with temperature of the PL intensity under Stokes and anti-Stokes excitation.

Fig. S6. Confocal maps of a 20 μm × 20 μm showing the PL signal from isolated nanodiamonds containing many GeV centers.

REFERENCES AND NOTES

1. V. Nathan, A. H. Guenther, S. S. Mitra, Review of multiphoton absorption in crystalline solids. *J. Opt. Soc. Am. A Opt. Image Sci. Vis.* **2**, 294–316 (1985).

2. H. Drexler, D. Leonard, W. Hansen, J. P. Kotthaus, P. M. Petroff, Spectroscopy of quantum levels in charge-tunable InGaAs quantum dots. *Phys. Rev. Lett.* **73**, 2252–2255 (1994).

3. D. W. Shipp, F. Sinjab, I. Notingher, Raman spectroscopy: Techniques and applications in the life sciences. *Adv. Opt. Photonics* **9**, 315–428 (2017).

4. T. M. Sweeney, S. G. Carter, A. S. Bracker, M. Kim, C. S. Kim, L. Yang, P. M. Vora, P. G. Brereton, E. R. Cleveland, D. Gammon, Cavity-stimulated Raman emission from a single quantum dot spin. *Nat. Photonics* **8**, 442–447 (2014).

5. R. I. Epstein, M. I. Buchwald, B. C. Edwards, T. R. Gosnell, C. E. Mungan, Observation of laser-induced fluorescent cooling of a solid. *Nature* **377**, 500–503 (1995).

6. C. L. Evans, E. O. Potma, M. Puoris'haag, D. Côté, C. P. Lin, X. S. Xie, Chemical imaging of tissue in vivo with video-rate coherent anti-Stokes Raman scattering microscopy. *Proc. Natl. Acad. Sci. U.S.A.* **102**, 16807–16812 (2005).

7. C. H. Camp Jr., M. T. Cicerone, Chemically sensitive bioimaging with coherent Raman scattering. *Nat. Photonics* **9**, 295–305 (2015).

8. Y. Xu, K. Naramoto, K. Narumi, K. Miyashita, T. Kamiya, T. Sakai, Strong anti-Stokes luminescence from H⁺–irradiated diamond. *Appl. Phys. Lett.* **83**, 1968–1970 (2003).

9. Q. Wang, Q. Zhang, X. Zhao, X. Luo, C. P. Y. Wong, J. Wang, D. Wan, T. Venkatesan, S. J. Pennycook, K. P. Loh, G. Eda, A. T. S. Wee, Photoluminescence upconversion by defects in hexagonal boron nitride. *Nano Lett.* **18**, 6898–6905 (2018).

10. M. W. Doherty, N. B. Manson, P. Delaney, F. Jelezko, J. Wrachtrup, L. C. L. Hollenberg, The nitrogen-vacancy colour centre in diamond. *Phys. Rep.* **528**, 1–45 (2013).

11. E. Neu, D. Steinmetz, J. Riedrich-Möller, S. Gsell, M. Fischer, M. Schreck, C. Becher, Single photon emission from silicon-vacancy colour centres in chemical vapour deposition nano-diamonds on iridium. *New J. Phys.* **13**, 025012 (2011).

12. M. K. Bhaskar, D. D. Sukachev, A. Sipahigil, R. E. Evans, M. J. Burek, C. T. Nguyen, L. J. Rogers, P. Siyushev, M. H. Metsch, H. Park, F. Jelezko, M. Lončar, M. D. Lukin, Quantum nonlinear optics with a germanium-vacancy color center in a nanoscale diamond waveguide. *Phys. Rev. Lett.* **118**, 223603 (2017).

13. G. Davies, Vibronic spectra in diamond. *J. Phys. C: Solid State Phys.* **7**, 3797 (1974).

14. R. Ulbricht, S. Dong, A. Gali, S. Meng, Z.-H. Loh, Vibrational relaxation dynamics of the nitrogen-vacancy center in diamond. *Phys. Rev. B* **97**, 220302 (2018).

15. K. N. Boldyrev, B. N. Mavrin, P. S. Sherin, M. N. Popova, Bright luminescence of diamonds with Ge-V centers. *J. Lumin.* **193**, 119–124 (2018).

16. E. Londero, G. Thiering, L. Razinkovas, A. Gali, A. Alkauskas, Vibrational modes of negatively charged silicon-vacancy centers in diamond from ab initio calculations. *Phys. Rev. B* **98**, 035306 (2018).

17. I. I. Vlasov, A. A. Shiryaev, T. Rendler, S. Steinert, S.-Y. Lee, D. Antonov, M. Vörös, F. Jelezko, A. V. Fisenko, L. F. Semjonova, J. Biskupek, U. Kaiser, O. I. Lebedev, I. Sildos, P. R. Hemmer, V. I. Konov, A. Gali, J. Wrachtrup, Molecular-sized fluorescent nanodiamonds. *Nat. Nanotechnol.* **9**, 54–58 (2014).

18. N. Aslam, G. Waldherr, P. Neumann, F. Jelezko, J. Wrachtrup, Photo-induced ionization dynamics of the nitrogen vacancy defect in diamond investigated by single-shot charge state detection. *New J. Phys.* **15**, 013064 (2013).

19. N. B. Manson, M. Hedges, M. S. J. Barson, R. Ahlefeldt, M. W. Doherty, M. J. Sellars, H. Abe, T. Ohshima, NV⁻–N⁺ pair centre in 1b diamond. arXiv:1807.08889 [cond-mat.mtrl-sci] (24 July 2018).

20. E. Neu, C. Hepp, M. Hauschild, S. Gsell, M. Fischer, H. Sternschulte, D. Steinmüller-Nethl, M. Schreck, C. Becher, Low-temperature investigations of single silicon vacancy colour centres in diamond. *New J. Phys.* **15**, 043005 (2013).

21. C. D. S. Brites, P. P. Lima, N. J. O. Silva, A. Millán, V. S. Amaral, F. Palacio, L. D. Carlos, Thermometry at the nanoscale. *Nanoscale* **4**, 4799–4829 (2012).

22. R. C. Maher, L. F. Cohen, J. C. Gallop, E. C. Le Ru, P. G. Etchegoin, Temperature-dependent anti-Stokes/Stokes ratios under surface-enhanced Raman scattering conditions. *J. Phys. Chem. B* **110**, 6797–6803 (2006).

23. C. T. Nguyen, R. E. Evans, A. Sipahigil, M. K. Bhaskar, D. D. Sukachev, V. N. Agafonov, V. A. Davydov, L. F. Kulikova, F. Jelezko, M. D. Lukin, All-optical nanoscale thermometry with silicon-vacancy centers in diamond. *Appl. Phys. Lett.* **112**, 203102 (2018).

24. J.-W. Fan, I. Cojocaru, J. Becker, I. V. Fedotov, M. H. A. Alkahtani, A. Alajlan, S. Blakley, M. Rezaee, A. Lyamkina, Y. N. Palyanov, Y. M. Borzdov, Y.-P. Yang, A. Zheltikov, P. Hemmer, A. V. Akimov, Germanium-vacancy color center in diamond as a temperature sensor. *ACS Photonics* **5**, 765–770 (2018).

25. M. Alkahtani, I. Cojocaru, X. Liu, T. Herzig, J. Meijer, J. Küpper, T. Lühmann, A. V. Akimov, P. R. Hemmer, Tin-vacancy in diamonds for luminescent thermometry. *Appl. Phys. Lett.* **112**, 241902 (2018).

26. G. Kucsko, P. C. Maurer, N. Y. Yao, M. Kubo, H. J. Noh, P. K. Lo, H. Park, M. D. Lukin, Nanometre-scale thermometry in a living cell. *Nature* **500**, 54–58 (2013).

27. J. F. Barry, M. J. Turner, J. M. Schloss, D. R. Glenn, Y. Song, M. D. Lukin, H. Park, R. L. Walsworth, Optical magnetic detection of single-neuron action potentials using quantum defects in diamond. *Proc. Natl. Acad. Sci. U.S.A.* **113**, 14133–14138 (2016).

28. T. Plakhotnik, H. Aman, H.-C. Chang, All-optical single-nanoparticle ratiometric thermometry with a noise floor of 0.3 K Hz⁻¹/². *Nanotechnology* **26**, 245501 (2015).

29. M. Mecklenburg, W. A. Hubbard, E. R. White, R. Dhall, S. B. Cronin, S. Aloni, B. C. Regan, Nanoscale temperature mapping in operating microelectronic devices. *Science* **347**, 629–632 (2015).

30. S. Li, K. Zhang, J.-M. Yang, L. Lin, H. Yang, Single quantum dots as local temperature markers. *Nano Lett.* **7**, 3102–3105 (2007).

31. H. Liu, Y. Fan, J. Wang, Z. Song, H. Shi, R. Han, Y. Sha, Y. Jiang, Intracellular temperature sensing: An ultra-bright luminescent nanothermometer with non-sensitivity to pH and ionic strength. *Sci. Rep.* **5**, 14879 (2015).

32. S. Kalytchuk, K. Poláková, Y. Wang, J. P. Froning, K. Cepe, A. L. Rogach, R. Zbořil, Carbon dot nanothermometry: Intracellular photoluminescence lifetime thermal sensing. *ACS Nano* **11**, 1432–1442 (2017).

33. Y. Tian, B. Tian, C. Cui, P. Huang, L. Wang, B. Chen, Size-dependent upconversion luminescence and temperature sensing behavior of spherical Gd₂O₃:Yb³⁺/Er³⁺ phosphor. *RSC Adv.* **5**, 14123–14128 (2015).

34. M. H. Alkahtani, C. L. Gomes, P. R. Hemmer, Engineering water-tolerant core/shell upconversion nanoparticles for optical temperature sensing. *Opt. Lett.* **42**, 2451–2454 (2017).

35. G. Jiang, S. Zhou, X. Wei, Y. Chen, C. Duan, M. Yin, B. Yang, W. Cao, 794 nm excited core–shell upconversion nanoparticles for optical temperature sensing. *RSC Adv.* **6**, 11795–11801 (2016).

36. X.-L. Chu, S. Götzinger, V. Sandoghdar, A single molecule as a high-fidelity photon gun for producing intensity-squeezed light. *Nat. Photonics* **11**, 58–62 (2017).

37. X. He, H. Htoon, S. K. Doorn, W. H. P. Pernice, F. Pyatkov, R. Krupke, A. Jeantet, Y. Chassagneux, C. Voisin, Carbon nanotubes as emerging quantum-light sources. *Nat. Mater.* **17**, 663–670 (2018).

38. C.-C. Fu, H.-Y. Lee, K. Chen, T.-S. Lim, H.-Y. Wu, P.-K. Lin, P.-K. Wei, P.-H. Tsao, H.-C. Chang, W. Fann, Characterization and application of single fluorescent nanodiamonds as cellular biomarkers. *Proc. Natl. Acad. Sci. U.S.A.* **104**, 727–732 (2007).

39. E. A. Ekimov, O. S. Kudryavtsev, N. E. Mordvinova, O. I. Lebedev, I. I. Vlasov, High-pressure synthesis of nanodiamonds from adamantane: Myth or reality? *ChemNanoMat* **4**, 269–273 (2018).

40. T. T. Tran, K. Kianinia, K. Bray, S. Kim, Z.-Q. Xu, A. Gentle, B. Sontheimer, C. Bradac, I. Aharonovich, Nanodiamonds with photostable sub-gigahertz linewidth quantum emitters. *APL Photonics* **2**, 116103 (2017).